Nanoscale

REVIEW

Cite this: *Nanoscale*, 2016, **8**, 3207

Strain engineering of graphene: a review

Chen Si,[a] Zhimei Sun[a] and Feng Liu*[b,c]

Received 5th November 2015,
Accepted 11th January 2016

DOI: 10.1039/c5nr07755a

www.rsc.org/nanoscale

Graphene has intrigued the science community by many unique properties not found in conventional materials. In particular, it is the strongest two-dimensional material ever measured, being able to sustain reversible tensile elastic strain larger than 20%, which yields an interesting possibility to tune the properties of graphene by strain and thus opens a new field called "straintronics". In this article, the current progress in the strain engineering of graphene is reviewed. We first summarize the strain effects on the electronic structure and Raman spectra of graphene. We then highlight the electron–phonon coupling greatly enhanced by the biaxial strain and the strong pseudomagnetic field induced by the non-uniform strain with specific distribution. Finally, the potential application of strain-engineering in the self-assembly of foreign atoms on the graphene surface is also discussed. Given the short history of graphene straintronics research, the current progress has been notable, and many further advances in this field are expected.

1. Introduction

Since its discovery in 2004,[1] graphene has attracted a great deal of attention. It is a two-dimensional (2D) sheet of sp^2-hybridized carbon atoms arranged like a honeycomb structure. In the 2D plane the strong σ bonds form the backbones of graphene, while the π bonds perpendicular to the plane form 2D electron gas with linear band dispersion near the Fermi level.[2] The unique lattice and electronic structures lead to many extraordinary properties of graphene, such as the giant intrinsic mobility of 2×10^5 cm^{-2} V^{-1} S^{-1} at room temperature,[3,4] very high thermal conductivity above 3000 W mK^{-1},[5] high transparency of 97.7%,[6] ability to sustain current densities a million times higher than that of copper[7] and impermeability to any gases.[8] These properties make graphene an ideal sample for the physical realization of many fundamental concepts and phenomena in solid state physics[9–11] as well as for the promising applications in electronics and optoelectronics.[12–15]

In the list of many remarkable properties of graphene, its mechanical properties are miraculous. Graphene is confirmed to be the strongest 2D material ever measured, with a Young's modulus of 1 TPa and an intrinsic strength of 130 GPa.[16] Most importantly, it is able to sustain reversible elastic tensile strain

[a]*School of Materials Science and Engineering, and Center for Integrated Computational Materials Engineering, International Research Institute for Multidisciplinary Science, Beihang University, Beijing 100191, China*
[b]*Department of Materials Science and Engineering, University of Utah, Salt Lake City, Utah 84112, USA. E-mail: fliu@eng.utah.edu*
[c]*Collaborative Innovation Center of Quantum Matter, Beijing 100084, China*

Chen Si

Chen Si is an assistant professor in the School of Materials Science and Engineering at Beihang University, China. She received her Ph.D. degree in Condensed Matter Physics from Tsinghua University in 2014. Her research interests are focused on the first-principles calculations of electronic properties and lattice dynamics of two-dimensional materials and topological insulators.

Zhimei Sun

Zhimei Sun is a Cheung Kong Scholar Chair Professor in the School of Materials Science and Engineering at Beihang University, China. She received her Ph.D. in Materials Science from the Institute of metal research, Chinese Academy of Sciences in 2002. She has been working in the research fields of semiconductors and high-performance structural materials with experience in both experiments and computational simulations.

as large as 25%,[16] while silicon typically breaks at the strain level of ~1.5%.[17] Experimentally, strains are expected to arise naturally in graphene. For example, graphene on a substrate usually experiences a moderate strain due to the surface corrugations of the substrate[18] or the lattice mismatch between graphene and the substrate.[19] On the other hand, there exists a maximum asymmetry in strain induced mechanical instability of graphene:[20] only less than 0.1% percent of compressive strain can be applied to a freestanding graphene of a typical sample size of micrometers. Inevitably, the relief of the compressive strain will lead to the formation of ripples and wrinkling.[20–22] Furthermore, intrinsic edge stress exists along the edges of graphene, rendering a mechanical edge twisting and warping instability.[23–25] Besides generated naturally, strain can also be intentionally induced and controlled in graphene by different techniques. Uniaxial strain can be induced by bending the flexible substrate on which graphene is elongated without slippage.[26,27] Biaxial strain can be introduced in graphene by three typical methods. The first method is directly using an atomic force microscopy (AFM) tip to push the graphene clamped on top of a hole fabricated in the substrate.[16] In the second method, graphene is transferred to a piezoelectric substrate, and the substrate is controllably shrank or elongated by applying a bias voltage, subjecting graphene to a uniform biaxial strain.[28] The third method is utilizing the thermal expansion mismatch between graphene and the underlying substrate to introduce strain in graphene.[29,30] Given that graphene has a negative thermal expansion coefficient, a substrate that has a positive thermal expansion coefficient, such as SiO_2,[30] can be intentionally selected. Then, by heating or cooling the substrate, the graphene will experience a tensile or compressive biaxial strain.[30]

The outstanding stretchability of graphene has driven graphene to be applied in flexible electronic devices, such as touch screens, electronic papers, and foldable organic light-emitting diodes (OLED)[12,31,32] as well as be used as construction materials as a pressure barrier[8] or graphene kirigami for building robust microscale structures with tunable mechanical properties.[33] On the other hand, it makes the strain engineering of graphene, *i.e.*, tuning the properties of graphene by mechanical strain, highly possible, which has led to a new field coined as "straintronics".[34–36] So far, a great number of fascinating physical phenomena of graphene induced by strain have been presented, such as the shifting of the Dirac cones,[37] the red shift and splitting of characteristic Raman modes,[26,38] the enhancement of the electron–phonon (e–ph) coupling,[39] the superconductivity,[39] the quantizing pseudomagnetic field[40] and the zero-field quantum hall effect.[41] In addition, strain is also proposed to be used for many potential applications.[42–47] For example, it can stabilize the metal-atom adsorption on graphene and prevent them from clustering;[42,43] and it can also increase the hydrogen coverage on graphene and assist their self-assembly.[44,45]

In this article, we attempt to give an up-to-date overview of the research progress in the strain engineering of graphene. We first review the strain effects on the electronic structure and Raman spectra of graphene. We then highlight the electron–phonon (e–ph) coupling greatly enhanced by the biaxial strain and the strong pseudomagnetic field induced by the non-uniform strain with specific distribution. We also discuss the application of the strain engineering in the self-assembly of foreign atoms on the graphene surface. Finally, we conclude the review with the outlook for the future.

2. Strain effects on the electronic structure of graphene

At equilibrium, the low-energy band structure of graphene can be approximated as cones located at the corners (K and K′ points) of the hexagonal Brillouin zone (BZ). In these cones (termed Dirac cones), the energy band dispersions are linear, and electrons and holes completely lose their effective mass. This linear band dispersion is a direct result of time reversal symmetry respected by the hexagonal lattice of graphene. It can be well described by a simple tight-binding (TB) model with electrons hopping only between the nearest-neighbor atoms and thus only one hopping parameter, $t_0 \approx 3$ eV, is required.[9,48]

The absence of the gap makes it difficult to find a direct application for graphene in electronics and optoelectronics. Hence the pursuit of a controllable gap in graphene has been a persistent goal for a long time. Various methods have been proposed or implemented to open a gap in graphene, such as size confinement,[49–51] graphene–substrate interactions,[52,53] surface adsorption,[54–56] and introducing specific defects.[57–59] Meanwhile, the effects of strain on the electronic structure of graphene have also attracted considerable attention, for taking advantage of bandgap engineering under large enough strain. Tight-binding models and *ab initio* calculations show that uniaxial strain shifts the Dirac cones away from K and K′ below a threshold strain value (~20%), but opens a gap above this threshold.[37,60–62] Similar behavior was found for a shear

Feng Liu

Feng Liu is a professor in the Department of Materials Science and Engineering at the University of Utah, a Fellow of the American Physical Society. He received his Ph.D. degree in Chemical Physics from Virginia Commonwealth University in 1990. His research interests lie in materials modeling and simulation from the atomic to mesoscopic scales, with a recent focus on the properties of surfaces and interfaces, growth mechanisms of thin films, and 2D materials, in particular surface-based 2D Dirac and topological materials.

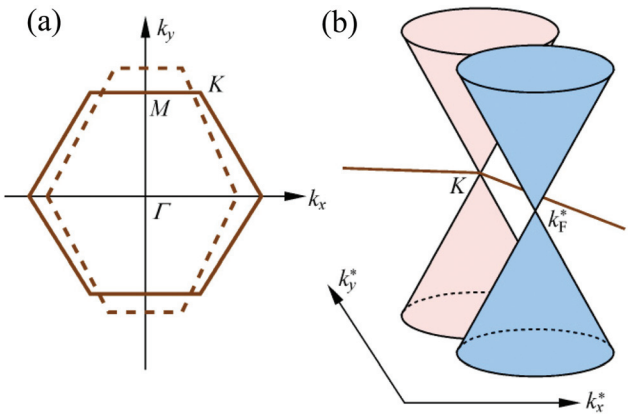

Fig. 1 Schematic illustrations of the effects of strain on graphene: (a) the deformation of the Brillouin zone; (b) the shifting of the Dirac cone away from the K point in the k^* space.[65] (Reprinted with permission from ref. 65. Copyright 2010 Springer.)

strain, but at a smaller threshold strain of ~16%.[63] Different from the uniaxial and shear strains, the biaxial strain preserves the crystal symmetry of graphene, thus neither shifts the Dirac points nor opens a gap, and instead changes the slope of the Dirac cones and hence the Fermi velocity.[60]

The shift of the Dirac cones under uniaxial or shear strain can be explained and quantitatively described by the theory developed by Yang and Han.[64,65] Consider the in-plane uniform deformation, described by a 2D strain tensor $\boldsymbol{\varepsilon} = (\varepsilon_{ij})_{2\times2}$. In the deformed graphene, real space vectors are $\boldsymbol{r} = (\boldsymbol{I} + \boldsymbol{\varepsilon})\boldsymbol{r}_0$, where $\boldsymbol{I}$ is the unit matrix and subscript "0" denotes the unstrained states. It is noted that after deformation the Brillouin zone (BZ) for the reciprocal vector $\boldsymbol{k}$ is not a regular hexagon any more, as shown in Fig. 1(a). However, if we introduce a $\boldsymbol{k}$ space transformation $\boldsymbol{k}^* = (\boldsymbol{I} + \boldsymbol{\varepsilon})^{\mathrm{T}}\boldsymbol{k}$, in the $\boldsymbol{k}^*$ space the BZ is restored to hexagonal as in the undeformed case, since $\boldsymbol{k}\cdot\boldsymbol{r} = \boldsymbol{k}\cdot(\boldsymbol{I} + \boldsymbol{\varepsilon})\boldsymbol{r}_0 = [(\boldsymbol{I} + \boldsymbol{\varepsilon})^{\mathrm{T}}\boldsymbol{k}]\cdot\boldsymbol{r}_0 = \boldsymbol{k}^*\cdot\boldsymbol{r}_0$. Then the TB Hamiltonian for the deformed graphene becomes

$$H(\boldsymbol{k}) = \sum_{j=1,2,3} t_j \exp(i\boldsymbol{k}\cdot\boldsymbol{a}_j) = \sum_{j=1,2,3} t_j \exp(i\boldsymbol{k}^*\cdot\boldsymbol{a}_{j0}). \quad (1)$$

Here, the sum is over j = 1,2,3 corresponding to three C–C bonds from a C atom with the vector $\boldsymbol{a}_j = (\boldsymbol{I} + \boldsymbol{\varepsilon})\boldsymbol{a}_0$ and bond length a_j; t_j is the hopping parameter dependent on the bond length a_j and can be expressed as $t_j = t_0(a_0/a_j)^2$ according to the Harrison hopping parameter relation. When the biaxial strain is imposed, t_1, t_2 and t_3 are equivalent, and the Fermi points, *i.e.*, the Dirac points, determined by solving $E(\boldsymbol{k}_F) = |H(\boldsymbol{k}_F)| = 0$, are exactly located at the corners of the hexagonal BZ, *i.e.*, the K and K′ points. When the uniaxial or shear strain is applied, t_1, t_2 and t_3 are no longer equivalent, thus the Fermi points will deviate from the K and K′ points. Let $\boldsymbol{k}_F^* = \boldsymbol{k}_K^* + \Delta\boldsymbol{k}_F^*$ ($\Delta\boldsymbol{k}_F^*$ denotes the deviation) and expand $|H(\boldsymbol{k}_F^*)| = 0$ to the first-order terms of $\boldsymbol{\varepsilon}$ and $\Delta\boldsymbol{k}_F^*$, then $\Delta\boldsymbol{k}_F^*$ is obtained to be[65]

$$\begin{cases} \Delta k_{Fx}^* = (1+\nu)\sigma\cos(3\theta) + \gamma\sin(3\theta) \\ \Delta k_{Fy}^* = -(1+\nu)\sigma\sin(3\theta) + \gamma\cos(3\theta) \end{cases} \quad (2)$$

where Δk_{Fx}^* and Δk_{Fy}^* are the components of $\Delta\boldsymbol{k}_F^*$ along the x and y direction, θ is the angle between the zigzag direction between the x-axis, σ is the uniaxial strain along the zigzag direction, γ is the shear strain, and ν is the Poisson's ratio. Similarly, one can get the deviation of the Dirac point from the K′ points, which is exactly opposite to that from the K point. Furthermore, by expanding $E(\boldsymbol{k}^*)$ near the Fermi points, the electron dispersion relation of the deformed graphene is obtained to be[65]

$$E\left(\boldsymbol{k}^*\right) = \pm\frac{3}{2}a_0 t_0\left|\boldsymbol{k}^* - \boldsymbol{k}_F^*\right| \quad (3)$$

From eqn (3) one can clearly see the effect of the uniaxial (or shear) strain on the electronic structure of graphene is shifting the Dirac cone in the $\boldsymbol{k}^*$ space, as shown in Fig. 1(b).

As mentioned above, under the uniaxial or shear strain, the Dirac cones located at points K and K′ are shifted in the opposite directions. So, if the uniaxial or shear strain is large enough, the two inequivalent Dirac points, which move away from the K and K′ points, respectively, may approach each other, and eventually merge, resulting in the opening of a realistic bandgap in graphene. This gap opening induced by the merging of the Dirac cones has been reported by several *ab initio* and TB calculations.[37,63,65,66] For a uniaxial strain along an arbitrary direction (except along the armchair direction), two inequivalent Dirac cones can always merge to open a gap when the strain is above a threshold value, and the zigzag direction is found to be the optimal direction which requires a smaller threshold strain (~23%).[37] For graphene under a shear strain, the merging of the Dirac cones and the gap opening appear at a shear strain of ~16%. When the shear strain is increased to 20%, the bandgap reaches to a maximum value of 0.72 eV.[63]

3. Strain dependence of the Raman spectra of graphene

Raman spectroscopy is widely considered as a key diagnostic tool for the graphene systems. It can identify the single layer graphene and give the information about doping, edges, defects and disorders.[67,68] Given that strain can effectively modify the electronic structure of graphene[60] and soften the optical-phonon branches,[69–71] it is expected to induce variations in Raman spectra. Fig. 2(a) shows the Raman spectra of a single layer graphene, which have two most intense features: one is the G band at 1580 cm^{-1}, and the other is the 2D band at ~2700 cm^{-1}.[67] Under the uniaxial strain, the G band redshifts and splits into two single bands, denoted by G^+ and G^-, respectively, according to their energies[26,38,72,73] [see Fig. 2(b)]. The splitting of the G band is originated from the reduction of the symmetry of graphene under the uniaxial strain. For the unstrained graphene, the G band arises from the doubly degenerate E_{2g} phonon mode at the Brillouin-zone center. When a uniaxial strain is imposed, the sixfold and threefold rotational symmetries of graphene are lost, and hence the E_{2g}

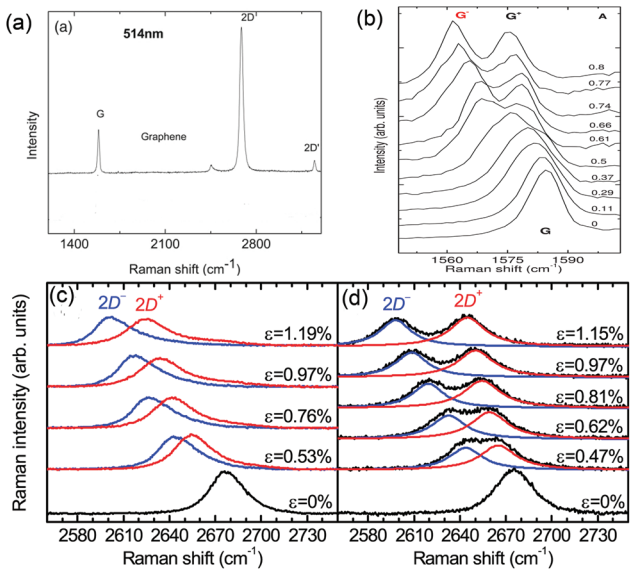

Fig. 2 (a) The Raman spectra of graphene measured at 514.5 nm.[67] (b) Evolution of the G band of graphene under the uniaxial strain.[72] (c), (d) Evolution of the 2D band under the uniaxial strain.[38] (c) is measured for the graphene sample which is stretched along the armchair direction, while (d) is for the graphene sample which is stretched along the zigzag direction. (Reprinted with permission from ref. 67, 72 and 38. Copyright 2007 Elsevier, Copyright 2009 American Physical Society and Copyright 2011 American Physical Society.)

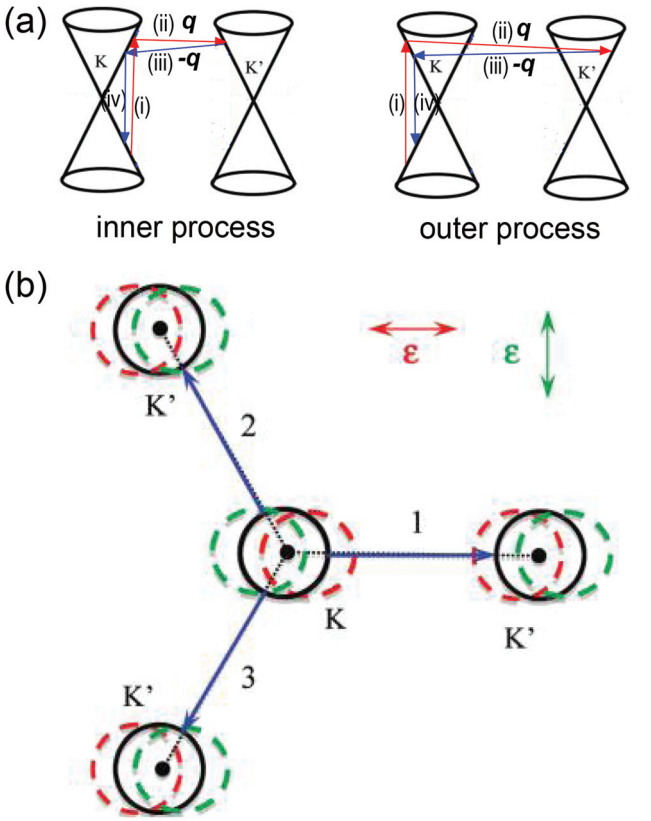

Fig. 3 (a) Double-resonance Raman scattering process for the 2D band (left: inner process, right: outer process). The process contains an electron–hole pair excitation induced by a laser (i), electron–phonon scattering with an exchanged momentum (***q*** or $-\boldsymbol{q}$) (ii and iii) and electron–hole recombination (iv). (b) Three Raman scattering paths (arrows labeled as 1, 2, and 3) from one Dirac cone (represented by a circle) at the K point to the three nearest Dirac cones at the K′ points. The dashed red (or green) circles indicate the movements of the Dirac cones when the graphene is stretched along the zigzag (or armchair) direction.[74] (Reprinted with permission from ref. 74. Copyright 2010 American Chemical Society.)

phonon mode splits into two singlet modes that give rise to the G^+ and G^- peaks, respectively.[26,72] In addition, the relative intensities of the G^+ and G^- peaks are found to depend strongly on the polarization direction of the incident light, which can be used to determine the angle between the strain direction and the graphene crystallographic orientation.[26,72]

Similar to the G band, the 2D band under the uniaxial strain also splits into two peaks, $2D^+$ and $2D^-$.[38,74] Both of them redshift as the strain increases, as shown in the Fig. 2(c) and (d) (Fig. 2(c) is for the uniaxial strain along the armchair direction, and Fig. 2(d) is for the uniaxial strain along the zigzag direction). It is noted that their frequency shift rates depend on the direction of the applied strain. In Yoon *et al.*'s work, for the graphene sample stretched along the armchair direction, the $2D^+$ and $2D^-$ shift rates are found to be -44.1 cm^{-1}/% and -63.1 cm^{-1}/%, respectively, whereas for the graphene sample stretched along the zigzag direction, these shift rates are -26.0 cm^{-1}/% and -67.8 cm^{-1}/%, respectively.[38] A similar strain direction dependence of shift rates for the $2D^+$ ($2D^-$) peak is also found by Huang *et al.*[74] although the values of shift rates are different, presumably because of the difference in the strain calibration.

The underlying mechanism for the strain-dependent variation of the 2D band was widely investigated.[38,74–76] It is now generally accepted that the splitting and redshift of the 2D band under the uniaxial strain are caused by the conspiracy of the Dirac cone shifting and the anisotropic phonon softening. It is known that the 2D band arises from the four-step double resonance Raman scattering as illustrated in Fig. 3(a): (i) a laser excites an electron–hole pair around a Dirac cone; (ii) the electron or hole is scattered inelastically to a neighboring Dirac cone by a phonon with momentum ***q***; (iii) the electron or hole is scattered back inelastically by another phonon with momentum $-\boldsymbol{q}$; (iv) the electron–hole recombines to emit a photon.[77,78] The resulting 2D Raman frequency is twice the frequency of the scattering phonon.[67] The scattering in progress (ii) and (iii), takes places between the Dirac cone at the K point and its three nearest neighbors at the K′ points (denoted as paths 1, 2, 3 in Fig. 3(b)), involving the smallest momentum transfer (inner process) and the largest momentum transfer (outer process).[74] And the inner process, which corresponds to the scattering of electrons or holes by the phonon from the TO branch between the Γ and K points, is verified to make a dominant contribution to the 2D band.[38,74,75] For unstrained graphene, the paths 1, 2, and 3 are completely equivalent, so that the 2D band appears as a single peak. Under the uniaxial

strain, as discussed in the section 2, the Dirac cones shift away from K and K′ points in opposite directions, which will directly induce variation in the scattering paths. Specifically, when the uniaxial strain is applied along the zigzag direction, the path 1 is shortened, while paths 2 and 3 are elongated; when strain is applied along the armchair direction, the path 1 is elongated, while the paths 2 and 3 are shortened. This is to say, under uniaxial strain the three equivalent scattering paths are divided into two types that involve scattering phonons with different momentum, rendering the 2D band to split into $2D^+$ and $2D^-$ bands.[74] In addition to the shifting of the Dirac cones, the optical phonons are also gradually softened due to the stretch of the C–C bonds as the uniaxial tensile strain increases. Especially, the softening of TO phonons associated with the $2D^+$ and $2D^-$ bands results in a redshift of the $2D^+$ and $2D^-$ bands. Moreover, *ab initio* calculations show that the softening rates of the TO phonons that satisfy the double-resonance conditions for the $2D^+$ and $2D^-$ Raman bands are significantly anisotropic, *i.e.*, they are sensitive to the direction of strain.[38] This is why the $2D^+$ ($2D^-$) band is shifted at different rates when the uniaxial strain is applied along different directions.

The effect of the biaxial strain on the Raman spectra was also investigated experimentally and theoretically.[28,75] Under the biaxial strain, all of the symmetries of graphene are preserved, and thus there is no splitting of the G and 2D bands. However, their red shifts are still observed,[28] due to the softening of the E_{2g} phonon associated with the G band and the TO phonon between the Γ and K points associated with the 2D band.

4. Strain-enhanced electron–phonon coupling in graphene

Although graphene has shown many remarkable properties, it is not superconducting. If it were possible to find a way to introduce superconductivity in graphene, it might enable more efficient integration of new device concepts, such as nanoscale superconducting quantum interference devices, superconducting transistors and single-electron superconductor–quantum dot devices. According to the Bardeen–Cooper–Schrieffer (BCS) theory,[79] the phonon-mediated superconductivity could be induced by an enhancement of e–ph coupling. By first-principles calculations, it has been shown that in combination with doping of electrons or holes, biaxial tensile strain can dramatically enhance the e–ph coupling of graphene so as to convert it into a BCS superconductor.[39]

The strength of e–ph coupling is characterized by a dimensionless parameter λ. In the intrinsic graphene, λ is very weak and superconductivity doesn't occur as the point-like Fermi surface leads to vanishing density of states (DOS). So the first step to increase λ is to increase the DOS at the Fermi level (N_F), which can be realized by doping with electrons or holes obviously. Fig. 4(a) shows the calculated N_F and λ as a function of hole doping concentration (n) for a p-type graphene.[39]

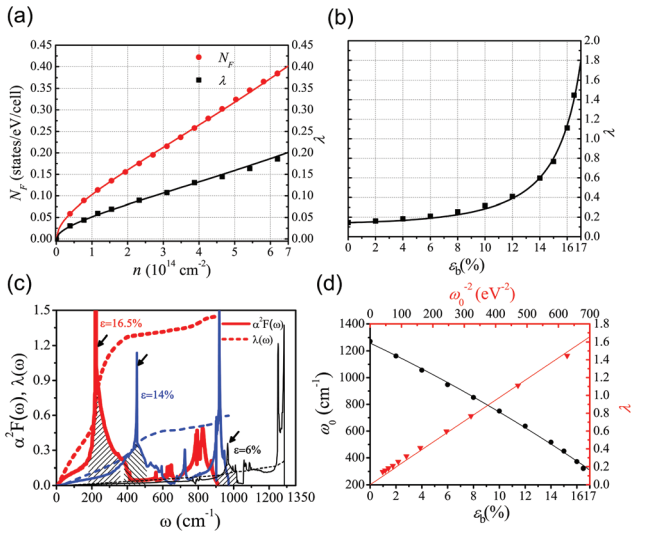

Fig. 4 (a) N_F and λ of hole doped graphene at different doping concentrations (n). λ *versus* biaxial strain ε_b (b) and Eliashberg spectral functions under 6%, 14% and 16.5% strains (c), the characteristic phonon frequency ω_0 *versus* ε_b (black dots) and ω_0^{-2} *versus* ε_b (red triangles) (d) for 4.65×10^{14} cm^{-2} hole doped graphene.[39] (Reprinted with permission from ref. 39. Copyright 2013 American Physical Society.)

Clearly, as n increases both N_F and λ increase, and $\lambda \approx 0.19$ at a high doping level of 6.2×10^{14} cm^{-2}, but still in the weak e–ph coupling regime. This indicates that doping is a necessary but insufficient condition to induce superconductivity in graphene. Very interestingly, it is further found that λ of doped graphene can be greatly enhanced by biaxial tensile strain (ε_b). Fig. 4(b) shows the calculated λ as a function of ε_b for a hole-doped graphene at a doping level of 4.65×10^{14} cm^{-2}, where one can clearly see that λ is strikingly increased with the strain in a non-linear fashion.[39] In particular, λ reaches as high as 1.45 at the strain of 16.5%, entering the strong coupling regime.

To understand such a dramatic enhancement of e–ph coupling triggered by strain, Fig. 4(c) shows the Eliashberg spectral function $\alpha^2F(\omega)$, which describes the mean coupling strength between the electrons with Fermi energy E_F and the phonons with frequency ω:

$$\alpha^2F(\omega) = \frac{1}{N_F N_k N_q}\sum_{mn}\sum_{q\nu}\delta(\omega-\omega_{q\nu}) \times \sum_{k}\left|g^{q\nu,mn}_{k+q,k}\right|^2\delta(E_{k+q,m}-E_F)\delta(E_{k,n}-E_F) \quad (4)$$

and the frequency-dependent e–ph coupling function

$$\lambda(\omega) = 2\int_0^{\omega}\frac{\alpha^2F(\omega')}{\omega'}d\omega' \quad (5)$$

where the electron with the energy eigenvalue E is indexed with momentum ($\boldsymbol{k}$) and the band index (m and n), the phonon with frequency ω is indexed with the momentum ($\boldsymbol{q}$) and the mode number (ν), and $g^{q\nu,mn}_{k+q,k}$ is the e–ph matrix

element.[80] It is seen that the Eliashberg function is sharply peaked at certain energy with a δ-like shape. For clarity, the peak that dominates the e–ph coupling is shaded. As the tensile strain increases, on the one hand, this peak moves toward lower energy, reflecting the softening of the corresponding optical phonon mode; on the other hand, the intensity of this peak is heightened. According to eqn (5), both of the redshift of the peak (decreasing ω) and the increase of the peak intensity (increasing $\alpha^2F(\omega)$) will increase λ.[39]

The above features of Eliashberg spectra of graphene suggest that strain-induced phonon softening plays a key role in the enhancement of λ. To establish their relationship, a characteristic phonon frequency (ω_0) is defined by averaging overall phonon frequencies weighted by the Eliashberg spectral function $\alpha^2F(\omega)$,

$$\omega_0 = \langle\omega^2\rangle^{1/2} = \sqrt{\int d\omega\omega\alpha^2F(\omega) / \int \frac{d\omega\alpha^2F(\omega)}{\omega}}. \quad (6)$$

Here, each phonon mode is weighted by its e–ph coupling strength, so that the calculated ω_0 represents the average phonon frequency contribution to λ. Fig. 4d shows ω_0 as a function of strain. Clearly, ω_0 decreases as ε_b increases. Also plotted in Fig. 4d is λ as a function of ${\omega_0}^{-2}$, illustrating a scaling relation of $\lambda \sim {\omega_0}^{-2}$. This relation provides a clear clue for us to understand the non-linear enhancement of λ under strain. By a theoretically model presented in ref. 39, one can further find two physical origins for this relation. One ${\omega_0}^{-1}$ is originated from the zero-point oscillation amplitudes of the phonons, *i.e.*, softer phonons resulting in larger deformation; the other ${\omega_0}^{-1}$ factor comes from the energy denominator in the perturbation theory for determining the electronic energy shift induced by the e–ph coupling, *i.e.*, softer phonons inducing stronger mixing between different electronic states around the Fermi surface.

An empirical function of $\lambda(n,\varepsilon_b)$ for the p-type graphene was also derived in ref. 39,

$$\lambda(n,\varepsilon_b) = \frac{\sqrt{n}}{11.93 - 2.19\sqrt{n}} \frac{0.5}{(1 - 0.007\varepsilon_b - 0.002{\varepsilon_b}^2)^2}. \quad (7)$$

By this function, one can simply estimate λ under different doping levels and strains. Fig. 5 shows the 3D plot of $\lambda(n, \varepsilon_b)$ using eqn (7). Some λ values directly calculated by first-principles (stars) are also shown and the two agree well.

The greatly enhanced e–ph coupling by the biaxial tensile strain suggests that the superconductivity can be induced in graphene. Using the McMillan–Allen–Dynes formula with a reasonable Coulomb pseudopotential μ^* = 0115, the critical transition temperature (T_c) for the superconducting state was estimated. It was found that when the biaxial strain exceeds 12%, the superconducting state may occur, and the T_c gradually increases with strain.[39] Taking the 1.55×10^{14}, 3.10×10^{14}, and 4.65×10^{14} cm^{-2} hole doped graphene as examples, at the tensile strain of 16.5%, their T_c remarkably reach as high as 18.6, 23.0, and 30.2 K, respectively.

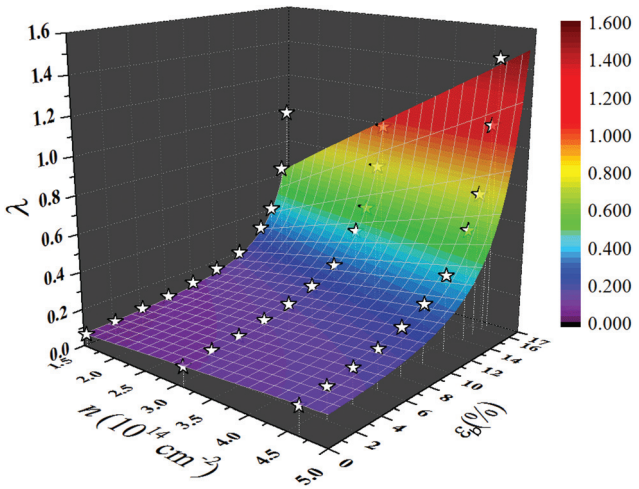

Fig. 5 3D plot of $\lambda(n, \varepsilon_b)$ calculated by eqn (7) and selected data (stars) calculated from first principles.[39] (Reprinted with permission from ref. 39. Copyright 2013 American Physical Society.)

It is widely known that experimental realization of the superconductivity in graphene has also attracted tremendous interest. The proximity-induced superconductivity was firstly observed in graphene by connecting it to a superconductor.[81,82] For example, the graphene monolayer grown directly on a superconducting Ru(0001) thin film shows a superconductive state below 2.1 K.[83] Recently, the doping-induced superconductivity in graphene has also been reported. Ludbrook *et al.* found that attaching a layer of Li atoms to monolayer graphene allows the material to achieve a stable, superconductive state below about 5.9 K.[84] Chapman *et al.* subsequently reported that Ca-decorated graphene becomes superconducting at about 6 K.[85] Herein, as reviewed above, the combination of doping and tensile biaxial strain offers an alternative route to strongly enhance the e–ph coupling of graphene and thus increase the superconducting transition temperature. On the one hand, the doping of graphene can be realized by adsorption of foreign atoms or by applying a gate voltage, with the resultant doping concentration being able to reach as large as 4×10^{14} cm^{-2} for both electrons and holes.[86] On the other hand, experimentally graphene can be elastically stretched up to ~25% tensile strain without breaking.[16] Therefore it is highly reasonable to expect experimental realization of high T_c superconducting graphene under the conspiracy of doping and strain. It is worth noting that the enhancement of the superconducting transition temperature by the tensile biaxial strain has been observed in MgB_2 films.[87]

5. Nonuniform strain induced pseudomagnetic field in graphene

A 2D strain distribution $\varepsilon_{ij}(x, y)$ results in the effective gauge field in graphene[88,89]

$$\boldsymbol{A} = \frac{\beta}{a}\begin{pmatrix} \varepsilon_{xx} - \varepsilon_{yy} \\ -2\varepsilon_{xy} \end{pmatrix} \quad (8)$$

where $a \approx 1.4$ Å is the lattice constant, $\beta = -\frac{\partial \ln t}{\partial \ln a} \approx 2$, $t \approx 3$ eV is the nearest-neighbor hopping parameter, and x-axis is chosen along the zigzag direction of graphene.[41] Evidently, a pseudomagnetic field B_s can be created by non-uniform strain, while the uniform strains considered in the section 2–4, including the biaxial strain (making $\boldsymbol{A} = 0$) and uniaxial strain (making $\boldsymbol{A}$ = constant), result in $B_s = 0$.

The existence of pseudomagnetic fields yields a possibility of creating such a strain distribution that gives rise to a strong uniform pseudomagnetic field, and, accordingly, leads to Landau quantization and a "pseudo-quantum Hall effect (QHE)" observable in zero magnetic field. One of such strain fields is proposed by F. Guinea *et al.*, with a strain pattern designed to align along three main crystallographic directions of graphene, having triangular symmetry.[41] It can generate a uniform quantizing B_s equivalent to tens of Tesla. For a finite doping, the strong B_s results in an insulting bulk state with the gap size $\delta E \approx 400K\sqrt{B_s}$ (>0.1 eV for $B_s = 10$ Tesla) and a pair of countercirculating edge states in the gap, similar to the case of a topological insulator. Later, it is predicted that, if a graphene ribbon is bent in-plane into a circular arc, it can also generate a strong gauge field that effectively acts as a uniform magnetic field larger than 10 Tesla.[90] On the one hand, this strong pseudomagnetic field in the graphene ribbon can lead to the formation of a well-defined transport gap on the order of 100 meV under a moderate strain of 10%; on the other hand, it can separate the electronic states from the two valleys in energy and in space, and thus establish the potential of graphene utilization in innovative electronics and valleytronics devices.[91]

The most striking experimental confirmation of the strain-induced pseudomagnetic field comes from the scanning tunneling microscopy (STM) of highly strained nanobubbles that form when graphene is grown on a Pt(111) surface.[40] Graphene on the Pt(111) has the minimum interaction with the substrate, compared with graphene on other transition metal substrates.[92] Graphene is not adhered to the Pt surface everywhere, and the nanobubbles frequently appear near the edge of the graphene patch, but are also sometimes observed in the center of flat patches or near the boundaries between the patches [see Fig. 6(a)]. These graphene nanobubbles are formed upon cooling, because of the mismatch in the expansion coefficients of the Pt substrate and graphene. Individual graphene nanobubbles often have a triangular shape, and they are typically 4–10 nm wide and 0.3 to 2.0 nm tall. Due to the large compressed strain, the lattice of graphene nanobubbles are distorted, but the honeycomb structure of graphene is maintained [see the inset of Fig. 6(a)]. Using the scanning tunneling spectroscopy (STS), the local electronic structures of strained graphene nanobubbles and surrounding graphene films are characterized, respectively, as shown in Fig. 6(b). STS measurements made directly over the nanobubble regions show a series of strong peaks spaced by more than 100 meV. It

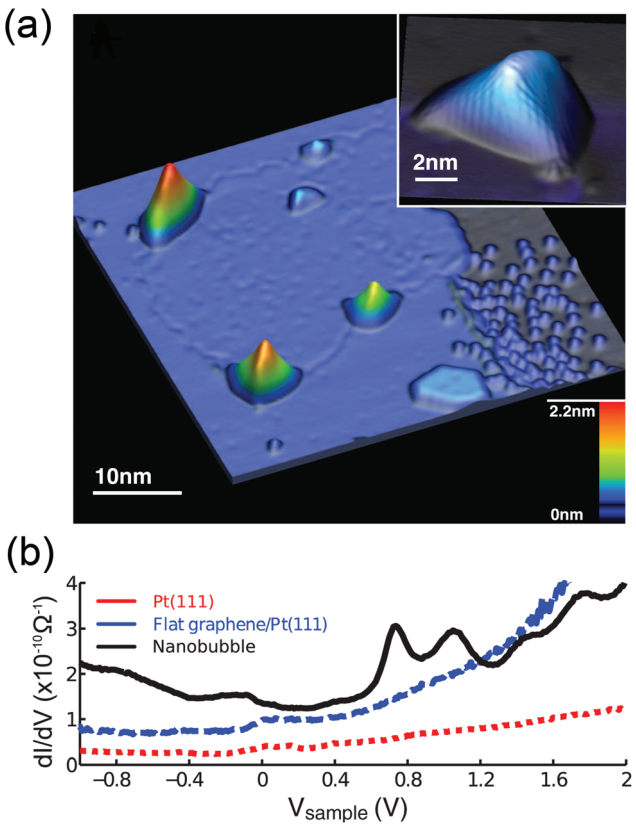

Fig. 6 (a) STM image of a graphene monolayer patch on the Pt(111) surface. There are four nanobubbles at the graphene–Pt border and one in the patch interior. (Inset) High-resolution image of a graphene nanobubble with distorted honeycomb lattice. (b) STS spectra of bare Pt(111), flat graphene on Pt(111) (shifted upward by 3×10^{-11} ohm^{-1}), and the center of a graphene bubble (shifted upward by 9×10^{-11} ohm^{-1}).[40] (Reprinted with permission from ref. 40. Copyright 2010 by the American Association for the Advancement of Science).

is noted that these peaks do not appear in the STS spectra of other regions. A careful study shows that the separation of these peaks is in the same way as the Landau levels in a magnetic field.[93] This means that these peaks arise from a large, relative uniform pseudomagnetic field induced by strain, which mimics the effects of the real magnetic field applied perpendicular to the graphene sheet and results in Landau quantization. By fitting the STS spectra by the magnetic field, the value of pseudomagnetic field B_s is determined to be 350 ± 40 Tesla. Such an enormous strain-induced pseudomagnetic field makes it possible to deliberately control the electronic properties of graphene through various schemes for applying strain and thus opens the door to design more novel electronic devices based on graphene.

6. Strain-engineered self-assembly of foreign atoms on the graphene surface

Surface adsorption has been considered as an effective strategy to tune the electronic and chemical properties of

graphene.[94,95] In particular, hydrogenation of graphene offers an elegant route towards opening the gap of graphene, and has been widely studied experimentally and theoretically.[54–56] However, the H adsorption on graphene is fundamentally a stochastic process, and directing H atoms to the exact locations as needed is not easy. Strain engineering is proposed to be a promising way to assist the self-assembly of adsorbed H atoms on graphene.[45] Compressive strain will induce protuberance or ripples in graphene,[96] and then the carbon atoms at the specific locations with a large curvature become more chemically reactive, acting as preferred sites for H adsorption.

Following this idea, a strain-engineered self-assembly process of H atoms on graphene is designed,[45] as shown in Fig. 7. The process consists of two steps. Starting with a pristine graphene sheet of length L (Fig. 7a), in the first step, a uniaxial compressive strain (ε_u) is applied along the x direction. Above a critical strain value, the flat graphene sheet becomes unstable, undulating into a 1D sinusoidal ripple pattern with period N_w [see Fig. 7b]. Based on a continuum mechanics model,[20] this critical strain is calculated to be $\varepsilon_{cr} = \frac{h^2 n^2 \pi^2}{12(1-\nu^2)L^2}$, where h = 0.7 Å (ref. 97) is the thickness of graphene, n is the number of ripple periods, and ν = 0.34 (ref. 98) is the Poisson's ratio. For the normal graphene size ($L \sim 10$–10^4 nm), the critical strain ε_{cr} is extremely small (<0.1%).[22] And for a given $L(\varepsilon_u)$, n increases as ε_u (L) increases. That is to say, the period of the ripple pattern (N_w) can be modulated by the length of graphene and the compressive strain. In the second step, the H atoms are introduced into the graphene nanoripple. They are preferred to adsorb on the C atoms with the largest curvature and then form a highly ordered H pattern [see Fig. 7c]. The higher reactivity of the curved C atoms is because, instead of the sp^2 electronic configuration in a planar symmetry, the curved C atom has a $sp^{2+\delta}$ configuration, which is closer to the final sp^3 configuration upon hydrogenation. Thus it costs less energy for H to adsorb on a curved C atom than on a planar C atom. The formed H stripes divide one ripple period into two ribbons, acting as a hard-wall potential to confine the π electrons between H stripes, and thus the graphene nanoripple behaves as the graphene nanoribbon and shows a realistic bandgap.

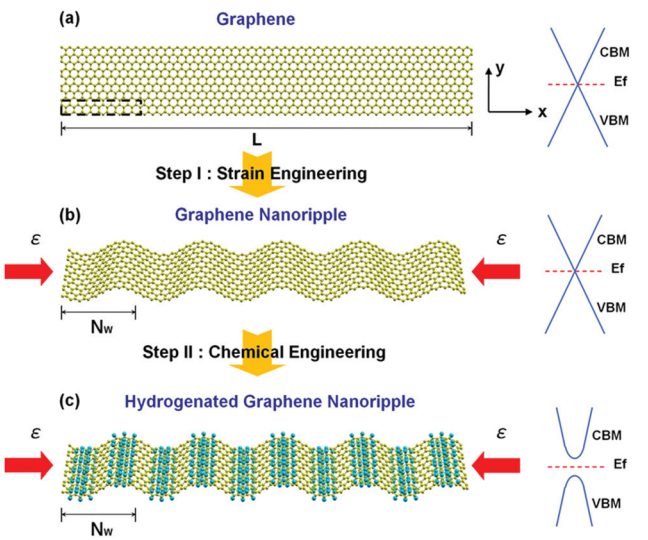

Fig. 7 Schematic illustration of the strain-engineered self-assembly process of H atoms on graphene.[45] (a) Pristine graphene with zero band gap. L denotes the length. (b) Graphene nanoripple formed by applying a compressive strain. ε_u and N_w is the compressive strain and the period of the nanoripple, respectively. (c) Directed adsorption of H atoms on the graphene nanoripple. In (b), the graphene remains semimetallic. In (c), after the directed H adsorption, the gap of graphene is opened. The CBM, VBM, E_f in (a), (b) and (c) denote the conduction band minimum, the valence band maximum and the Fermi level, respectively. (Reprinted with permission from ref. 45. Copyright 2011 American Physical Society.)

It is noted that this strain-engineered approach for the self-assembly of H atoms has some evident advantages. First, the H atoms are directed by the strain-induced nanoripple template to the designed locations with the largest curvature, instead of random adsorption sites, which results in the formation of the hydrogenated graphene nanostripe with a uniform width, orientation, smooth edges and a non-zero bandgap. Second, the magnitude of compressive strain can tune the width of the graphene nanostripe, and hence the eventual bandgap. Third, the self-assembly process is repeatable, and a cycle of directed H adsorption (desorption) at (from) the same surface locations leads to a reversible metal–semiconductor–metal transition with the same bandgap.

Experimentally, as a first step towards strain-based engineering, controlled graphene ripples have been well achieved for suspended graphene using thermally generated strains,[96] for substrate-supported graphene by substrate regulation,[99] and for graphene on a pre-stretched elastomeric substrate by controlling the relaxation of the pre-strains.[100,101] Then the controlled graphene ripples can be used to direct the self-assembly of H adatoms as demonstrated above. Similarly, this idea also applies to the self-assembly of other adatoms such as F, Cl and O on graphene. In particular, graphene oxide, one of the most studied chemically modified forms of graphene, shows a range of oxygen functionalized groups randomly adsorbing on the graphene surface when it is synthesized *via* a commonly used aggressive acidic treatment developed by Hummers and Offeman.[102] However, when it is produced by oxidizing epitaxial graphene on SiC(0001) using atomic oxygen under ultrahigh vacuum,[103] due to the inevitable formation of ripples in the epitaxial graphene[104] the adsorbed O atoms would prefer to occupy the specific sites with the largest local curvature to realize a self-assembly.

7. Conclusions and outlook

In this article, we have reviewed the effects of strain on the properties of graphene, and discussed the potential applications of the strain engineering of graphene. Uniform uniaxial or shear strain shifts the Dirac cones of graphene away from K and K′ points of the Brillouin zone in opposite directions,

but does not open a gap in graphene when it is smaller than the threshold value (>20% for uniaxial strain and 16% for the shear strain). When it is larger than the threshold value, the gap can be opened due to the merging of the Dirac cones. Another way to introduce a gap in graphene is to design the specific non-uniform strain distribution that can generate a strong quantizing pseudomagnetic field and, consequently, result in Landau quantization and a QHE-like state. At a finite doping, graphene will change from semimetallic to semiconducting if the Fermi level lies between the Landau levels. Apart from the change of the electronic structure, the dependence of Raman spectra on strain is also briefly reviewed, such as the red shift and splitting of both the G band and the 2D band under uniaxial strain. Consequently, Raman spectroscopy has been used as a key diagnostic tool to monitor the strain, including the sign and direction of strain. We also highlight the effects of biaxial strain on the e–ph coupling of graphene. Biaxial tensile stain can greatly enhance the e–ph coupling by softening the optical phonon modes, and even induce superconductivity in graphene. Finally, we have discussed the potential application of strain-engineering in the self-assembly of foreign atoms on the graphene surface. By applying a compressive strain on flat graphene to form graphene nanoripples, the adsorbed atoms, such as H atoms, are directed to the designed locations with the largest curvature, instead of random adsorption sites.

Strain engineering opens the door to both fundamental study of more novel physical phenomena in graphene and exploration of more efficient integration of a variety of promising device concepts. At the same time, as an effective means to tune the properties of materials, it is being implemented to other 2D materials,[105–108] such as transition metal dichalcogenides and phosphorene, due to the outstanding flexibility of these materials like that of graphene.[109,110] Usually, similar techniques to induce strain in graphene are also applicable to other 2D materials.[17] One exciting finding worth mentioning is that strain can dramatically modulate the bandgap of some 2D semiconductors, and thus their electronic and optoelectronic performance.[106,111–113] For instance, single layer MoS_2 subjected to uniform (uniaxial or biaxial) tensile strain shows its bandgap linearly decreasing with increasing tensile strain, first undergoing a direct to indirect bandgap transition and then a semiconductor to metal transition;[114,115] and the change of the bandgap directly results in variation of the photoluminescence spectra.[112] Given the short history and the large pool of 2D materials,[116–118] the field of strain engineering in 2D materials is still in its infancy, and further developments in this field are expected to occur in the near future.

Acknowledgements

C. Si and Z. Sun acknowledge support by the National Natural Science Foundation for Distinguished Young Scientists of China (51225205) and the National Natural Science Foundation of China (11504015, 61274005). F. Liu acknowledges support by U.S. DOE-BES (Grant No. DE-FG02-04ER46148). C. Si also acknowledges support by the open research fund program of the state key laboratory of low-dimensional quantum physics (KF201508).

Notes and references

1 K. S. Novoselov, A. K. Geim, S. Morozov, D. Jiang, Y. Zhang, S. A. Dubonos, I. Grigorieva and A. Firsov, *Science*, 2004, **306**, 666–669.
2 D. Abergel, V. Apalkov, J. Berashevich, K. Ziegler and T. Chakraborty, *Adv. Phys.*, 2010, **59**, 261–482.
3 A. S. Mayorov, R. V. Gorbachev, S. V. Morozov, L. Britnell, R. Jalil, L. A. Ponomarenko, P. Blake, K. S. Novoselov, K. Watanabe and T. Taniguchi, *Nano Lett.*, 2011, **11**, 2396–2399.
4 S. Morozov, K. Novoselov, M. Katsnelson, F. Schedin, D. Elias, J. Jaszczak and A. Geim, *Phys. Rev. Lett.*, 2008, **100**, 016602.
5 A. A. Balandin, *Nat. Mater.*, 2011, **10**, 569–581.
6 R. Nair, P. Blake, A. Grigorenko, K. Novoselov, T. Booth, T. Stauber, N. Peres and A. Geim, *Science*, 2008, **320**, 1308–1308.
7 J. Moser, A. Barreiro and A. Bachtold, Current-induced cleaning of graphene, *Appl. Phys. Lett.*, 2007, **91**, 163513.
8 J. S. Bunch, S. S. Verbridge, J. S. Alden, A. M. van der Zande, J. M. Parpia, H. G. Craighead and P. L. McEuen, *Nano Lett.*, 2008, **8**, 2458–2462.
9 A. C. Neto, F. Guinea, N. Peres, K. S. Novoselov and A. K. Geim, *Rev. Mod. Phys.*, 2009, **81**, 109.
10 N. Peres, *Rev. Mod. Phys.*, 2012, **82**, 2673.
11 X. Chen, Y. Liu, B.-L. Gu, W. Duan and F. Liu, *Phys. Rev. B: Condens. Matter*, 2014, **90**, 121403.
12 K. S. Novoselov, V. Fal, L. Colombo, P. Gellert, M. Schwab and K. Kim, *Nature*, 2012, **490**, 192–200.
13 R. Sun, Y. Zhang, K. Li, C. Hui, K. He, X. Ma and F. Liu, *Appl. Phys. Lett.*, 2013, **103**, 013106.
14 L. P. Biró, P. Nemes-Incze and P. Lambin, *Nanoscale*, 2012, **4**, 1824–1839.
15 Z. Wang and F. Liu, *Nanoscale*, 2011, **3**, 4201–4205.
16 C. Lee, X. Wei, J. W. Kysar and J. Hone, *Science*, 2008, **321**, 385–388.
17 R. Roldán, A. Castellanos-Gomez, E. Cappelluti and F. Guinea, 2015, arXiv:1504.07926.
18 M. Teague, A. Lai, J. Velasco, C. Hughes, A. Beyer, M. Bockrath, C. Lau and N.-C. Yeh, *Nano Lett.*, 2009, **9**, 2542–2546.
19 Z. Ni, W. Chen, X. Fan, J. Kuo, T. Yu, A. Wee and Z. Shen, *Phys. Rev. B: Condens. Matter*, 2008, **77**, 115416.
20 Y. Zhang and F. Liu, *Appl. Phys. Lett.*, 2011, **99**, 241908.
21 M. S. Bronsgeest, N. Bendiab, S. Mathur, A. Kimouche, H. T. Johnson, J. Coraux and P. Pochet, *Nano Lett.*, 2015, **15**, 5098–5104.
22 G. Sun, J. Jia, Q. Xue and L. Li, *Nanotechnol.*, 2009, **20**, 355701.

23 B. Huang, M. Liu, N. Su, J. Wu, W. Duan, B.-L. Gu and F. Liu, *Phys. Rev. Lett.*, 2009, **102**, 166404.
24 V. Shenoy, C. Reddy, A. Ramasubramaniam and Y. Zhang, *Phys. Rev. Lett.*, 2008, **101**, 245501.
25 N. Su, M. Liu and F. Liu, *Nano Res.*, 2011, **4**, 1242–1247.
26 M. Huang, H. Yan, C. Chen, D. Song, T. F. Heinz and J. Hone, *Proc. Natl. Acad. Sci. U. S. A.*, 2009, **106**, 7304–7308.
27 T. Yu, Z. Ni, C. Du, Y. You, Y. Wang and Z. Shen, *J. Phys. Chem. C*, 2008, **112**, 12602–12605.
28 F. Ding, H. Ji, Y. Chen, A. Herklotz, K. Dörr, Y. Mei, A. Rastelli and O. G. Schmidt, *Nano Lett.*, 2010, **10**, 3453–3458.
29 N. Ferralis, R. Maboudian and C. Carraro, *Phys. Rev. Lett.*, 2008, **101**, 156801.
30 D. Yoon, Y.-W. Son and H. Cheong, *Nano Lett.*, 2011, **11**, 3227–3231.
31 K. S. Kim, Y. Zhao, H. Jang, S. Y. Lee, J. M. Kim, K. S. Kim, J.-H. Ahn, P. Kim, J.-Y. Choi and B. H. Hong, *Nature*, 2009, **457**, 706–710.
32 Y. Shao, M. F. El-Kady, L. J. Wang, Q. Zhang, Y. Li, H. Wang, M. F. Mousavi and R. B. Kaner, *Chem. Soc. Rev.*, 2015, **44**, 3639–3665.
33 M. K. Blees, A. W. Barnard, P. A. Rose, S. P. Roberts, K. L. McGill, P. Y. Huang, A. R. Ruyack, J. W. Kevek, B. Kobrin, D. A. Muller and L. McEuen, *Nature*, 2015, **524**, 204–207.
34 V. M. Pereira and A. C. Neto, *Phys. Rev. Lett.*, 2009, **103**, 046801.
35 D. Zhan, J. Yan, L. Lai, Z. Ni, L. Liu and Z. Shen, *Adv. Mater.*, 2012, **24**, 4055–4069.
36 G. G. Naumis and P. Roman-Taboada, *Phys. Rev. B: Condens. Matter*, 2014, **89**, 241404.
37 V. M. Pereira, A. C. Neto and N. Peres, *Phys. Rev. B: Condens. Matter*, 2009, **80**, 045401.
38 D. Yoon, Y.-W. Son and H. Cheong, *Phys. Rev. Lett.*, 2011, **106**, 155502.
39 C. Si, Z. Liu, W. Duan and F. Liu, *Phys. Rev. Lett.*, 2013, **111**, 196802.
40 N. Levy, S. Burke, K. Meaker, M. Panlasigui, A. Zettl, F. Guinea, A. C. Neto and M. Crommie, *Science*, 2010, **329**, 544–547.
41 F. Guinea, M. Katsnelson and A. Geim, *Nat. Phys.*, 2010, **6**, 30–33.
42 M. Zhou, Y. Lu, C. Zhang and Y. P. Feng, *Appl. Phys. Lett.*, 2010, **97**, 103109.
43 O. Cretu, A. V. Krasheninnikov, J. A. Rodríguez-Manzo, L. Sun, R. M. Nieminen and F. Banhart, *Phys. Rev. Lett.*, 2010, **105**, 196102.
44 M. L. Ng, R. Balog, L. Hornekær, A. Preobrajenski, N. A. Vinogradov, N. Mårtensson and K. Schulte, *J. Phys. Chem. C*, 2010, **114**, 18559–18565.
45 Z. Wang, Y. Zhang and F. Liu, *Phys. Rev. B: Condens. Matter*, 2011, **83**, 041403.
46 S.-H. Bae, Y. Lee, B. K. Sharma, H.-J. Lee, J.-H. Kim and J.-H. Ahn, *Carbon*, 2013, **51**, 236–242.
47 B. Huang, J. Yu and S.-H. Wei, *Phys. Rev. B: Condens. Matter*, 2011, **84**, 075415.
48 Z. Wang and F. Liu, *ACS Nano*, 2010, **4**, 2459–2465.
49 M. Y. Han, B. Özyilmaz, Y. Zhang and P. Kim, *Phys. Rev. Lett.*, 2007, **98**, 206805.
50 Y.-W. Son, M. L. Cohen and S. G. Louie, *Phys. Rev. Lett.*, 2006, **97**, 216803.
51 Q. Yan, B. Huang, J. Yu, F. Zheng, J. Zang, J. Wu, B.-L. Gu, F. Liu and W. Duan, *Nano Lett.*, 2007, **7**, 1469–1473.
52 S. Zhou, G.-H. Gweon, A. Fedorov, P. First, W. De Heer, D.-H. Lee, F. Guinea, A. C. Neto and A. Lanzara, *Nat. Mater.*, 2007, **6**, 770–775.
53 M. S. Nevius, M. Conrad, F. Wang, A. Celis, M. N. Nair, A. Taleb-Ibrahimi, A. Tejeda and E. H. Conrad, *Phys. Rev. Lett.*, 2015, **115**, 136802.
54 D. Elias, R. Nair, T. Mohiuddin, S. Morozov, P. Blake, M. Halsall, A. Ferrari, D. Boukhvalov, M. Katsnelson and A. Geim, *Science*, 2009, **323**, 610–613.
55 A. K. Singh and B. I. Yakobson, *Nano Lett.*, 2009, **9**, 1540–1543.
56 R. Balog, B. Jørgensen, L. Nilsson, M. Andersen, E. Rienks, M. Bianchi, M. Fanetti, E. Lægsgaard, A. Baraldi and S. Lizzit, *Nat. Mater.*, 2010, **9**, 315–319.
57 W. Liu, Z. Wang, Q. Shi, J. Yang and F. Liu, *Phys. Rev. B: Condens. Matter*, 2009, **80**, 233405.
58 F. Ouyang, S. Peng, Z. Liu and Z. Liu, *ACS Nano*, 2011, **5**, 4023–4030.
59 D. Yu, E. M. Lupton, M. Liu, W. Liu and F. Liu, *Nano Res.*, 2008, **1**, 56–62.
60 S.-M. Choi, S.-H. Jhi and Y.-W. Son, *Phys. Rev. B: Condens. Matter*, 2010, **81**, 081407.
61 M. Farjam and H. Rafii-Tabar, *Phys. Rev. B: Condens. Matter*, 2009, **80**, 167401.
62 R. Ribeiro, V. M. Pereira, N. Peres, P. Briddon and A. C. Neto, *New J. Phys.*, 2009, **11**, 115002.
63 G. Cocco, E. Cadelano and L. Colombo, *Phys. Rev. B: Condens. Matter*, 2010, **81**, 241412.
64 L. Yang and J. Han, *Phys. Rev. Lett.*, 2000, **85**, 154–157.
65 Y. Li, X. Jiang, Z. Liu and Z. Liu, *Nano Res.*, 2010, **3**, 545–556.
66 F. Pellegrino, G. Angilella and R. Pucci, *Phys. Rev. B: Condens. Matter*, 2010, **81**, 035411.
67 A. C. Ferrari, *Solid State Commun.*, 2007, **143**, 47–57.
68 M. S. Dresselhaus, A. Jorio, M. Hofmann, G. Dresselhaus and R. Saito, *Nano Lett.*, 2010, **10**, 751–758.
69 C. A. Marianetti and H. G. Yevick, Failure mechanisms of graphene under tension, *Phys. Rev. Lett.*, 2010, **105**, 245502.
70 C. Si, W. Duan, Z. Liu and F. Liu, *Phys. Rev. Lett.*, 2012, **109**, 226802.
71 F. Liu, P. Ming and J. Li, *Phys. Rev. B: Condens. Matter*, 2007, **76**, 064120.
72 T. M. G. Mohiuddin, A. Lombardo, R. R. Nair, A. Bonetti, G. Savini, R. Jalil, N. Bonini, D. M. Basko, C. Galiotis, N. Marzari, K. S. Novoselov, A. K. Geim and A. C. Ferrari, *Phys. Rev. B: Condens. Matter*, 2009, **79**, 205433.

73 Z. H. Ni, T. Yu, Y. H. Lu, Y. Y. Wang, Y. P. Feng and Z. X. Shen, *ACS Nano*, 2008, **2**, 2301–2305.
74 M. Huang, H. Yan, T. F. Heinz and J. Hone, *Nano Lett.*, 2010, **10**, 4074–4079.
75 M. Mohr, J. Maultzsch and C. Thomsen, *Phys. Rev. B: Condens. Matter*, 2010, **82**, 201409.
76 O. Frank, M. Mohr, J. Maultzsch, C. Thomsen, I. Riaz, R. Jalil, K. S. Novoselov, G. Tsoukleri, J. Parthenios and K. Papagelis, *ACS Nano*, 2011, **5**, 2231–2239.
77 A. Ferrari, J. Meyer, V. Scardaci, C. Casiraghi, M. Lazzeri, F. Mauri, S. Piscanec, D. Jiang, K. Novoselov and S. Roth, *Phys. Rev. Lett.*, 2006, **97**, 187401.
78 C. Thomsen and S. Reich, *Phys. Rev. Lett.*, 2000, **85**, 5214.
79 J. Bardeen, L. N. Cooper and J. R. Schrieffer, *Phys. Rev.*, 1957, **106**, 162.
80 G. Grimvall, *The electron–phonon interaction in metals*, North-Holland, Amsterdam, 1981.
81 A. Shailos, W. Nativel, A. Kasumov, C. Collet, M. Ferrier, S. Guéron, R. Deblock and H. Bouchiat, *Europhys. Lett.*, 2007, **79**, 57008.
82 H. B. Heersche, P. Jarillo-Herrero, J. B. Oostinga, L. M. Vandersypen and A. F. Morpurgo, *Nature*, 2007, **446**, 56.
83 C. Tonnoir, A. Kimouche, J. Coraux, L. Magaud, B. Delsol, B. Gilles and C. Chapelier, *Phys. Rev. Lett.*, 2013, **111**, 246805.
84 B. Ludbrook, G. Levy, P. Nigge, M. Zonno, M. Schneider, D. Dvorak, C. Veenstra, S. Zhdanovich, D. Wong and P. Dosanjh, *Proc. Natl. Acad. Sci. U. S. A.*, 2015, **112**, 11795.
85 J. Chapman, Y. Su, C. Howard, D. Kundys, A. Grigorenko, F. Guinea, A. Geim, I. Grigorieva and R. Nair, 2015, arXiv:1508.06931.
86 D. K. Efetov and P. Kim, *Phys. Rev. Lett.*, 2015, **105**, 256805.
87 A. Pogrebnyakov, J. Redwing, S. Raghavan, V. Vaithyanathan, D. Schlom, S. Xu, Q. Li, D. Tenne, A. Soukiassian and X. Xi, *Phys. Rev. Lett.*, 2004, **93**, 147006.
88 H. Suzuura and T. Ando, *Phys. Rev. B: Condens. Matter*, 2002, **65**, 235412.
89 J. L. Manes, *Phys. Rev. B: Condens. Matter*, 2007, **76**, 045430.
90 F. Guinea, A. Geim, M. Katsnelson and K. Novoselov, *Phys. Rev. B: Condens. Matter*, 2010, **81**, 035408.
91 T. Low and F. Guinea, *Nano Lett.*, 2010, **10**, 3551–3554.
92 M. Gao, Y. Pan, C. Zhang, H. Hu, R. Yang, H. Lu, J. Cai, S. Du, F. Liu and H.-J. Gao, *Appl. Phys. Lett.*, 2010, **96**, 053109.
93 D. L. Miller, K. D. Kubista, G. M. Rutter, M. Ruan, W. A. de Heer, P. N. First and J. A. Stroscio, *Science*, 2009, **324**, 924–927.
94 Q. Tang, Z. Zhou and Z. Chen, *Nanoscale*, 2013, **5**, 4541–4583.
95 P. Lehtinen, A. Foster, A. Ayuela, A. Krasheninnikov, K. Nordlund and R. Nieminen, *Phys. Rev. Lett.*, 2003, **91**, 017202.
96 W. Bao, F. Miao, Z. Chen, H. Zhang, W. Jang, C. Dames and C. N. Lau, *Nat. Nanotechnol.*, 2009, **4**, 562–566.
97 Z.-C. Tu and Z.-C. Ou-Yang, *Phys. Rev. B: Condens. Matter*, 2002, **65**, 233407.
98 J. Zang, O. Aldas-Palacios and F. Liu, *Comput Phys. Commun.*, 2007, **2**, 451–465.
99 T. Li and Z. Zhang, *J. Phys. D: Appl. Phys.*, 2010, **43**, 075303.
100 Y. Wang, R. Yang, Z. Shi, L. Zhang, D. Shi, E. Wang and G. Zhang, *ACS Nano*, 2011, **5**, 3645–3650.
101 J. Zang, S. Ryu, N. Pugno, Q. Wang, Q. Tu, M. J. Buehler and X. Zhao, *Nat. Mater.*, 2013, **12**, 321–325.
102 D. R. Dreyer, S. Park, C. W. Bielawski and R. S. Ruoff, *Chem. Soc. Rev.*, 2010, **39**, 228–240.
103 M. Z. Hossain, J. E. Johns, K. H. Bevan, H. J. Karmel, Y. T. Liang, S. Yoshimoto, K. Mukai, T. Koitaya, J. Yoshinobu and M. Kawai, *Nat. Chem.*, 2012, **4**, 305–309.
104 F. Varchon, P. Mallet, J.-Y. Veuillen and L. Magaud, *Phys. Rev. B: Condens. Matter*, 2008, **77**, 235412.
105 X. Sui, C. Si, B. Shao, X. Zou, J. Wu, B.-L. Gu and W. Duan, *J. Phys. Chem. C*, 2015, **119**, 10059–10063.
106 K. He, C. Poole, K. F. Mak and J. Shan, *Nano Lett.*, 2013, **13**, 2931–2936.
107 C. Si, J. Liu, Y. Xu, J. Wu, B.-L. Gu and W. Duan, *Phys. Rev. B: Condens. Matter*, 2014, **89**, 115429.
108 M. Zhou, W. Duan, Y. Chen and A. Du, *Nanoscale*, 2015, **7**, 15168–15174.
109 S. Bertolazzi, J. Brivio and A. Kis, *ACS Nano*, 2011, **5**, 9703–9709.
110 Q. Wei and X. Peng, *Appl. Phys. Lett.*, 2014, **104**, 251915.
111 A. Rodin, A. Carvalho and A. C. Neto, *Phys. Rev. Lett.*, 2014, **112**, 176801.
112 H. J. Conley, B. Wang, J. I. Ziegler, R. F. Haglund Jr., S. T. Pantelides and K. I. Bolotin, *Nano Lett.*, 2013, **13**, 3626–3630.
113 N. Lu, H. Guo, L. Li, J. Dai, L. Wang, W.-N. Mei, X. Wu and X. C. Zeng, *Nanoscale*, 2014, **6**, 2879–2886.
114 E. Scalise, M. Houssa, G. Pourtois, V. Afanas'ev and A. Stesmans, *Nano Res.*, 2012, **5**, 43–48.
115 P. Lu, X. Wu, W. Guo and X. C. Zeng, *Phys. Chem. Chem. Phys.*, 2012, **14**, 13035–13040.
116 B. Dubertret, T. Heine and M. Terrones, *Acc. Chem. Res.*, 2015, **48**, 1–2.
117 C. Si, J. Zhou and Z. Sun, *ACS Appl. Mater. Interfaces*, 2015, **7**, 17510–17515.
118 H. Zhang, *ACS Nano*, 2015, **9**, 9451–9469.